Japanese Journal of Applied Physics **54**, 063001 (2015) **REGULAR PAPER**
http://dx.doi.org/10.7567/JJAP.54.063001

Faraday effect of bismuth iron garnet thin film prepared by mist CVD method

Situ Yao[1]*, Takafumi Sato[1], Kentaro Kaneko[2], Shunsuke Murai[1], Koji Fujita[1], and Katsuhisa Tanaka[1]

[1]*Department of Material Chemistry, Graduate School of Engineering, Kyoto University, Kyoto 615-8510, Japan*
[2]*Photonics and Electronics Science and Engineering Center, Kyoto University, Kyoto 615-8520, Japan*
E-mail: yao@dipole7.kuic.kyoto-u.ac.jp

Received January 26, 2015; accepted April 5, 2015; published online May 18, 2015

Metastable bismuth iron garnet (BIG, an abbreviation of $Bi_3Fe_5O_{12}$), one kind of garnet-type ferrites, is known to manifest very large Faraday rotation as well as low optical absorption in the visible to infrared region. We report on successful synthesis of thin film composed of single-phase BIG epitaxially grown on single-crystalline gadolinium gallium garnet ($Gd_3Ga_5O_{12}$, GGG) substrate by using mist chemical vapor deposition (CVD) method, which is an emerging technique for preparation of thin films. The crystal structure, surface morphology, and magnetic, optical and magneto-optical properties of the resultant thin films have been explored. The BIG thin film has a relatively flat surface free from roughness compared to those prepared by other vapor deposition methods. Saturation magnetization is about 1620 G at room temperature, which is close to that expected from the ideal magnetic structure of BIG. The maximum value of Faraday rotation angle reaches 54.3 deg/μm at a wavelength of 424 nm. This value is rather large when compared with those reported for BIG thin films prepared by other techniques. The wavelength dependence of Faraday rotation angle is analyzed well in terms of the crystal electric field (CEF) level schema. Our result suggests that the mist CVD method is a simple and effective technique to synthesize BIG thin film with excellent magneto-optical properties.

1. Introduction

Garnet-type ferrites, the composition of which is denoted by $R_3Fe_5O_{12}$ with R usually being rare-earth element, have attracted considerable attention because of their magnetic properties and functionalities that are of interest as well as importance from both fundamental and practical viewpoints, including recent finding related to the spin Hall effect.[1,2] In particular, materials based on the garnet-type ferrites such as $Y_3Fe_5O_{12}$ (YIG) and $Gd_3Fe_5O_{12}$ (GIG) have been utilized as an optical isolator in a wavelength range around 1.5 μm for optical telecommunications. Not only large Faraday effect but also low optical absorption achieved in those garnet-type ferrites is of great importance in the application to the optical isolator. It is known that large trivalent cations such as Bi^{3+} can replace the rare-earth ions in the garnet-type ferrites and that the replacement by Bi^{3+} significantly enhances the Faraday effect while it keeps the optical absorption still low.[3] For example, $x = 1.25$ composition in $Y_{3-x}Bi_xFe_5O_{12}$ manifests Faraday rotation 20 times larger than that of YIG at a wavelength of 0.52 μm.[4] Also, magneto-optical figure of merit is larger by one order of magnitude for $Gd_2BiFe_5O_{12}$ than for YIG in a wavelength range from 0.7 to 1.0 μm.[5] The enhancement of Faraday effect by the incorporation of Bi^{3+} originates in the strong spin–orbital interaction of the 6p orbital of Bi^{3+} ion.[6] Nonetheless, it is impossible to replace all the rare-earth ions in a garnet-type ferrite by Bi^{3+} ions as far as the stable phase of the garnet-type ferrites is concerned.[7,8] For instance, the composition of Bi-substituted GIG in which the concentration of Bi^{3+} ion incorporated is maximized is $Gd_{1.6}Bi_{1.4}Fe_5O_{12}$.[7] On the other hand, $Bi_3Fe_5O_{12}$ (BIG), i.e., the garnet-type ferrite with all the rare-earth ions being replaced by Bi^{3+} ions, can exist as a metastable phase, as firstly demonstrated by Okuda et al.[9] They succeeded in synthesis of BIG thin film by using reactive ion beam (RIB) sputtering. Since the discovery of metastable BIG phase with garnet-type structure, several kinds of methods including RF sputtering, electron cyclotron resonance (ECR) sputtering, pulsed laser deposition (PLD), and metal–organic decomposition (MOD) have been carried out to synthesize BIG thin films.[10–13)]

Among many methods for preparation of oxide thin films through gas or liquid phase, mist chemical vapor deposition (CVD) is one of the emerging techniques and is anticipated to be a low-cost, large-area, and industrial-scale process. In fact, the mist CVD method does not require any vacuum chambers and the procedure is rather simple; as long as reagents can be dissolved in solvents and ultrasonically atomized, thin film can be grown efficiently and homogeneously under atmospheric pressure. This technique was first developed for preparation of large-scale zinc oxide (ZnO) thin film without vacuum apparatus.[14] Since then, thin films of more than twenty kinds of metal oxides have been prepared by utilizing this method.[15,16] In the previous study, we successfully synthesized YIG thin film, a prototype of garnet-type ferrite as described above, by using the mist CVD method.[17] We could obtain dense and homogeneous thin films with excellent magnetic and magneto-optical properties, suggesting that the mist CVD method is also effective for obtaining high quality thin films of multiple oxides. Besides, the mist CVD process has advantages of high deposition rate and small fluctuation in composition. Moreover, inevitable incorporation of Pb^{2+} into garnet-type ferrite prepared by liquid phase epitaxy (LPE) method, which stems from the use of flux containing Pb^{2+} and is an origin to decrease the transmittance of the ferrite,[18,19] can be avoided when the mist CVD method is carried out. This is because highly pure bismuth and iron compounds can be used as starting materials in the mist CVD process.

In the present study, we have synthesized BIG thin film by means of the mist CVD method. Neither large surface roughness nor morphology composed of three-dimensional (3D) islands reported for BIG thin films prepared by physical vapor deposition (PVD) method[20,21] is observed in the films prepared by the mist CVD method. The present mist CVD-derived BIG thin films possess flat surfaces in virtue of the crystal growth from liquid phase and show large Faraday rotation angle as well as high saturation magnetization presumably because the preparation process in air can suppress the formation of oxygen vacancies.

2. Experimental procedure

BIG thin films were grown on (111)-oriented gadolinium gallium garnet (GGG) substrates by using a fine-channel type mist sourced film former (TOUKI MSFF-FC). Before the deposition, the substrates were cleaned by ultrasonic cleaning process in a potassium hydroxide (KOH)–water (H_2O)–isopropyl alcohol (IPA) solution to remove residue of slurry used for polishing of surfaces of the substrates and then annealed at 1000 °C for 3 h to improve the crystallinity. Various kinds of conventional solvents were put to the test for the preparation of BIG thin films, and consequently, *N*,*N*-dimethylformamide (DMF) was found to be the most appropriate among all the solvents tested. In particular, water was inadequate because Bi could be hardly found in the deposited thin films when aqueous solution was used. Thus, the precursor solution was prepared by dissolving tris(acetylacetonato)iron(III), $Fe(C_5H_8O_3)_3$ in DMF and mixing it with 2-ethylhexanoic acid solution containing 25 wt% of bismuth(III) 2-ethylhexanoate, $Bi(C_8H_{15}O_2)_3$. DMF solutions with different molar ratios of $Bi(C_8H_{15}O_2)_3$ to $Fe(C_5H_8O_3)_3$ (hereafter, referred to as [Bi]/[Fe]) were prepared, while the total concentration of [Bi] + [Fe] was kept to be 0.050 mol/L.

The precursor solution was ultrasonically atomized by using a 2.4 MHz transducer, and the mist droplets were transferred to the reaction vessel with nitrogen gas at a flow rate of 6 L/min, 3 L/min of which was to carry the mist of atomized precursor solution (called carrier gas) and the other 3 L/min to assist the smooth flow of the mist (called dilution gas). The substrate temperature was set above 300 °C at which evaporation of the solvent and decomposition of the metal sources were completed according to the result of thermogravimetric analysis, and thereby no organic residues remained in the deposited thin films on the substrate. Because the as-deposited thin film grown at 300 °C was amorphous, post-annealing was carried out. As mentioned below, single-phase of BIG was grown by the post-annealing at 530 °C for 30 min.

The crystal structure of the thin films was analyzed by using X-ray diffraction (XRD) with Cu Kα radiation. The film thickness was mainly determined by a high-sensitivity surface profiler with a diamond tip. So as to measure the film thickness by the surface profiler, the substrate was partly covered with a cover glass plate 0.12 mm thick during the deposition process. Because the film thickness is of decisive importance in the characterization of magneto-optical properties, it was also estimated from the cross-sectional image obtained by field emission scanning electron microscopy (FE-SEM). The composition of the thin films was determined by Rutherford backscattering spectrometry (RBS) using a 2 MeV He^+ beam, which was produced by a Pelletron-type accelerator of the Quantum Science and Engineering Center heavy ion accelerator facility of Kyoto University. Based on the analysis of the measured Rutherford backscattering spectra, the film thickness was also calculated. It should be noted that the values of thickness evaluated by surface profiler, FE-SEM, and RBS are in agreement with each other. The surface morphology of the thin films was observed by atomic force microscopy (AFM). The oxidation state of iron ion in the BIG thin films was evaluated by means of X-ray photoelectron spectroscopy (XPS).

Magnetic field dependence of magnetization for the present BIG thin films was measured at room temperature by using a superconducting quantum interference device magnetometer (SQUID). First, magnetization of a GGG substrate was measured and then BIG thin film was deposited on the substrate. Secondly, magnetization of the sample composed of BIG thin film and GGG substrate was measured, and the data obtained for the GGG substrate was subtracted. Optical transmittance measurements were carried out at room temperature by using ultraviolet–visible–infrared spectrophotometry in a wavelength range from 200 to 2000 nm. Faraday rotation angle was measured by a polarization modulation technique with a xenon lamp as a light source. The thin film sample was placed in a static magnetic field of 15 kOe applied in a direction perpendicular to the surface of the thin film, and rotation angle was measured in a wavelength range from 350 to 850 nm at room temperature. Non-negligible effect of paramagnetic GGG substrate was eliminated by subtracting the data for only the GGG substrate from those of the sample composed of BIG thin film and the substrate.

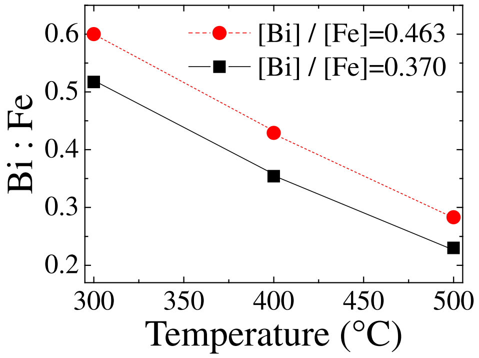

Fig. 1. (Color online) Molar ratio of Bi to Fe in thin films deposited at varied substrate temperatures. Precursor solutions with different molar ratios of Bi to Fe, i.e., [Bi]/[Fe] = 0.463 and 0.370, were used for the thin film deposition. All the thin films were post-annealed at 530 °C for 30 min.

3. Results and discussion

3.1 Synthesis of BIG thin film by the mist CVD method

First we explored the effect of synthesis conditions including the molar ratio of Bi to Fe in the precursor solution, substrate temperature, and post-annealing temperature on the composition and crystalline phases of the resultant thin films. Figure 1 shows the molar ratio of Bi to Fe in the post-annealed thin films obtained by the RBS as a function of the substrate temperature as well as the molar ratio of Bi to Fe in the precursor solution, i.e., [Bi]/[Fe]. For those thin films, the post-annealing was carried out at 530 °C for 30 min. It is found that the molar ratio of Bi to Fe in the thin film deposited on the substrate at 300 °C is larger than the value of [Bi]/[Fe], suggesting that the deposition rate is higher for Bi-associated chemical species than for Fe-associated one at this temperature. The molar ratio of Bi to Fe in the thin films gradually decreases with an increase in the substrate temperature and becomes smaller than the value of [Bi]/[Fe] at the substrate temperature of 500 °C. This means that the activation energy for the deposition process is lower for the Bi-associated chemical species than for the Fe-associated one, although the details of the reaction mechanism to yield the oxide thin film, i.e., the thermal decomposition of precursors containing the metal elements and the subsequent deposition as oxide, are not clear at this moment. Figure 1 also indicates that the composition of the thin film can be tuned by

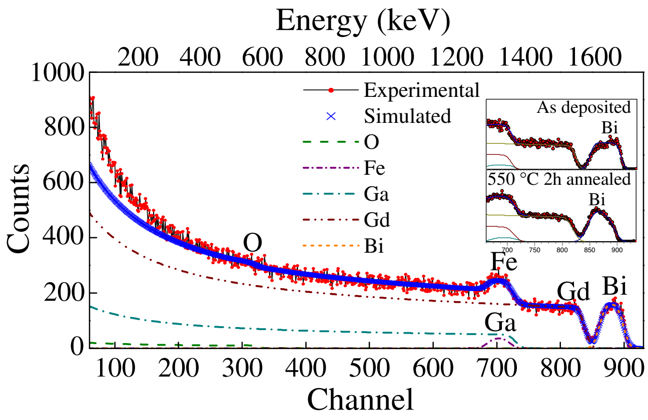

Fig. 2. (Color online) RBS signals of BIG thin film deposited at 300 °C and post-annealed at 530 °C for 30 min. The inset shows RBS signals of as-deposited and long-time annealed BIG thin films for comparison. The long-time annealing was performed at 550 °C for 2 h.

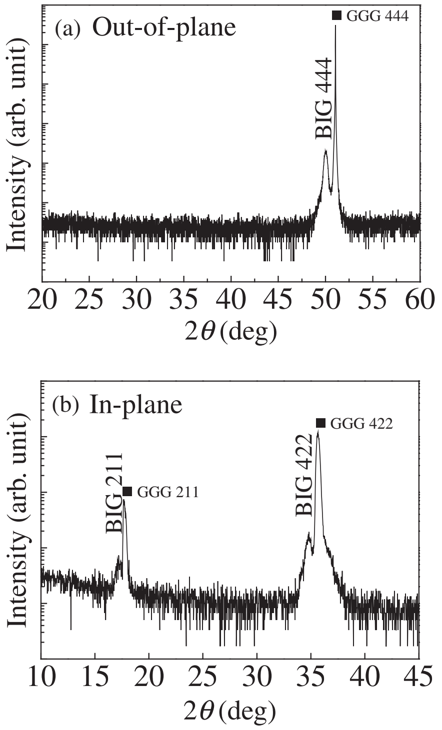

Fig. 3. (a) Out-of-plane and (b) in-plane XRD patterns of BIG thin film grown on (111)-orientated GGG substrate. Deposition was carried out at 300 °C from the precursor solution with [Bi]/[Fe] of 0.463 and the resultant thin film was post-annealed at 530 °C for 30 min.

adjusting the synthesis conditions, although the substrate temperature higher than 500 °C leads to the formation of stable crystalline phases, i.e., $BiFeO_3$ and $Bi_2Fe_4O_9$. Figure 2 illustrates the result of RBS for the thin film deposited at 300 °C and post-annealed at 530 °C for 30 min. The thin film was deposited from the precursor solution with [Bi]/[Fe] of 0.463. From the analysis of signals of each constituent atoms, it is found that the molar ratio of Bi to Fe in the thin film is 0.600, which is consistent with the stoichiometric composition of BIG. The insets of Fig. 2 display the results of RBS for thin film as-deposited at 300 °C and that obtained by post-annealing the as-deposited thin film at 550 °C for 2 h. The analyses of the data illustrated in the insets reveal that the molar ratios of Bi to Fe in the thin films are 0.655 and 0.505, respectively, for the as-deposited and post-annealed thin films. In other words, the as-deposited thin film possesses excess Bi and oppositely the thin film post-annealed at 550 °C for 2 h is short of Bi compared with the stoichiometric composition. The post-annealing at higher temperatures for longer duration is apt to make the composition Bi-deficient because bismuth oxide is volatile.

XRD analysis was carried out for thin films deposited at 300 °C from the precursor solution with [Bi]/[Fe] of 0.463 and post-annealed at varied temperatures for 30 min (the data are not shown). The as-deposited thin film is amorphous, and the precipitation of BIG begins at an annealing temperature of 500 °C. The XRD lines assigned to BIG become more intense as the post-annealing temperature is increased, but BIG is decomposed to result in the formation of $BiFeO_3$ and $Bi_2Fe_4O_9$ as the post-annealing temperature becomes 550 °C. Figure 3 shows out-of-plane (a) and in-plane (b) XRD patterns of the thin film obtained by post-annealing at 530 °C for 30 min after deposited on the (111)-oriented GGG substrate at 300 °C. Only diffraction lines ascribable to BIG and GGG are found; in particular, only 444 diffraction lines of both BIG and GGG appear in the out-of-plane pattern, and only 211 and 422 diffraction lines are observed in the in-plane pattern due to the in-plane orientations. These facts indicate that the BIG thin film was epitaxially grown on the GGG substrate when the deposition was carried out at a substrate temperature of 300 °C and the resultant amorphous thin film was post-annealed at 530 °C for 30 min. The lattice parameter of the epitaxial BIG thin film has been determined by plotting lattice parameters evaluated from the present 2θ peak positions shown in Figs. 3(a) and 3(b) against the Nelson–Riley function: $(\cos^2\theta/\sin\theta) + (\cos^2\theta/\theta)$, and by extrapolation of this relation to $2\theta = 180°$.[22] The lattice parameter is obtained as $a = 12.630$ Å, for which the coefficient of determination, $R^2 = 0.9998$. This value of lattice parameter is in excellent agreement with reported ones.[23–25] Hereafter, we focus on the single-phase BIG thin film obtained under these conditions.

The surface of the BIG thin film observed by AFM is illustrated in Fig. 4. The AFM image discloses that the present epitaxial BIG thin film has a relatively flat surface when compared with BIG thin films prepared by PVD methods. The 3D island morphology observed for PLD-derived BIG thin film is not found in the present thin film.[20,21] The standard deviation of surface roughness evaluated from the AFM measurement is 1.103 nm, an order of magnitude smaller than BIG thin films grown by PLD method.[26,27] The result reflects superiority of the mist CVD method. Namely, this method supplies a flow of mist droplets to assure that surface of the substrate can be covered evenly and continuously by liquidus or gaseous precursors. A more important point is that a substrate is placed in a very narrow reaction vessel, called fine-channel, which forces precursor droplets to move toward the substrate. The detailed physics for the deposition process in the mist CVD method was reviewed by Kawaharamura.[28]

The valence state of Fe was examined by using XPS. The XPS peaks of Fe $2p_{3/2}$ and Fe $2p_{1/2}$ are shown in Fig. 5. Different oxidation states of Fe can be distinguished by comparing the peak position and the shape of the satellite

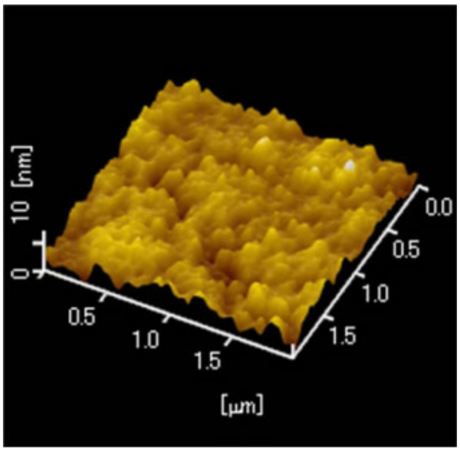

Fig. 4. (Color online) AFM image of BIG thin film epitaxially grown on (111)-orientated GGG substrate.

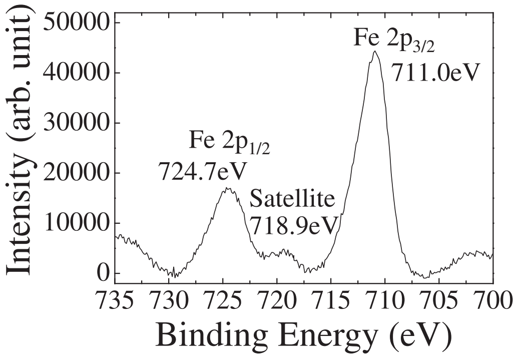

Fig. 5. XPS of Fe 2p for the BIG thin film epitaxially grown on (111)-orientated GGG substrate.

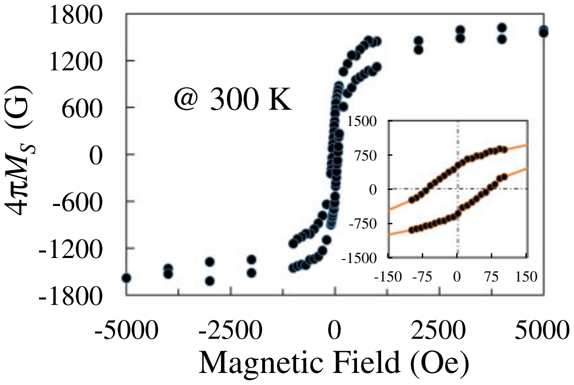

Fig. 6. (Color online) Room temperature magnetization as a function of magnetic field for the BIG thin film epitaxially grown on (111)-orientated GGG substrate. The inset shows an enlarged view in the low field range.

peak with those of standard samples such as Fe_2O_3 and Fe_2SiO_4. The binding energies of Fe $2p_{3/2}$ and Fe $2p_{1/2}$ estimated from Fig. 5 are 711.0 and 724.7 eV, respectively. The satellite peak of Fe $2p_{3/2}$, which is located 7.9 eV higher than $2p_{3/2}$ peak, is clearly observed. According to the values of binding energy provided by Yamashita,[29] it is found that the iron ions in the present BIG thin film prepared by the mist CVD method are present as trivalent state.

3.2 Magnetic, optical, and magneto-optical properties

A unit cell of BIG consists of 8 chemical formula units and contains 24 dodecahedral, 16 octahedral, and 24 tetrahedral sites. Fe^{3+} ions reside octahedral and tetrahedral sites in a molar ratio of 2 to 3, and magnetic moments on these sites align antiparallel due to superexchange coupling between them, leading to ferrimagnetism. The ferrimagnetism lasts at temperatures much higher than room temperature, as indicated by the Curie temperature experimentally obtained for BIG, although the value is diverse ranging from 618 to 701 K most likely owing to the deficiency or excess of Bi.[10,30–33] Also, Curie temperature of BIG extrapolated from the data of Bi-substituted YIG is 672 K.[34] Figure 6 shows room temperature magnetization as a function of external magnetic field for the present BIG thin film. The magnetization is saturated at low magnetic fields, and a hysteresis loop is clearly observed (in the inset of Fig. 6), indicating that the present BIG thin film exhibits ferrimagnetic behavior at room temperature. Typical values of the saturation magnetization $4\pi M_S$ reported for BIG thin films derived by the PVD methods range from 1200 to 1500 G.[23–25] There is a tendency that BIG thin films grown from liquidus phase have higher saturation magnetization. For instance, $4\pi M_S$ of BIG thin film prepared by MOD method was reported to be 1700 G, very close to a value expected for ideal magnetic structure of BIG; the magnetic structure of BIG as mentioned above is thought to be very similar to that of YIG and $4\pi M_S$ equals 1760 G for single-crystalline bulk YIG.[35,36] For the present thin film, the magnetization reaches about 1620 G. Similarly to MOD method, the mist CVD method is thought to suppress the formation of oxygen vacancies because the reaction proceeds in air, and consequently, all the Fe ions present as the trivalent state, as demonstrated by the XPS data, leading to the high value of M_S.[17]

Not only the magnetization but optical absorption is an important factor to evaluate the practical performance of magneto-optical materials such as BIG. The optical transmittance spectrum of the epitaxial BIG thin film 230 nm thick is given as open circles in Fig. 7(a). Interference fringes are clearly observed, confirming that the present BIG thin film is free from surface roughness with a rather homogeneous thickness. The transmittance is slightly higher than that of PLD-derived BIG thin film 220 nm thick,[42] i.e., a thin film with a thickness almost the same as the present thin film. It should be noted that no external magnetic field was applied when the transmittance was measured, and consequently, light scattering by magnetic domain walls may affect the transmittance. For a two-layer system composed of a single layer thin film on a thick finite transparent substrate, the optical transmittance can be described by the Swanepoel formula.[37] The spectrum calculated by the formula is shown as a solid curve in Fig. 7(a), and the agreement between experimental and calculated transmittance spectra is excellent although the surface roughness of the BIG thin film is not considered in the calculation. Calculations which took into account the surface roughness as standard deviation of thickness, σ_d, were performed in the analysis of transmittance for thick or rough BIG films.[26,38,39] In other words, $\sigma_d = 0$ in the present case, indicating that the surface roughness of the BIG thin film prepared by the mist CVD method is not very significant. The dispersion of refractive index, i.e., $n(\lambda) = 2.42 + (310/\lambda)^2$, and the dispersion of extinction coefficient,

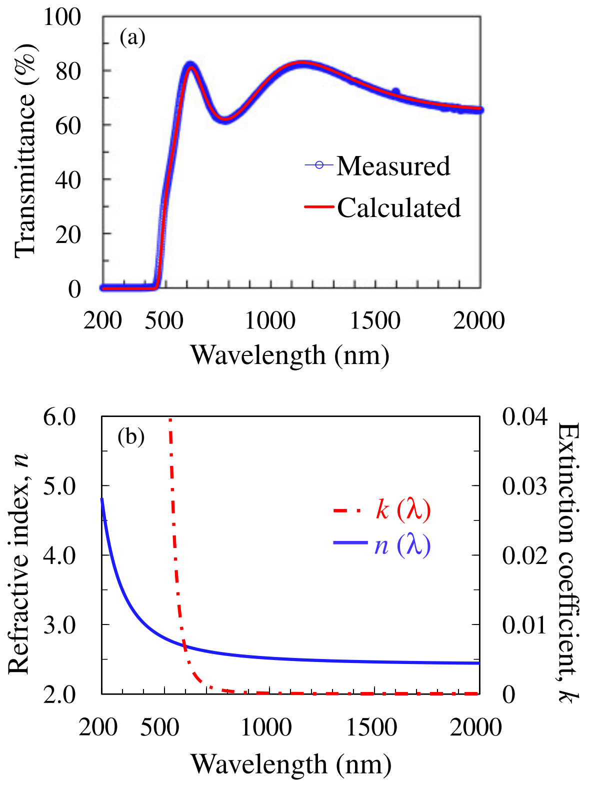

Fig. 7. (Color online) (a) Optical transmittance spectrum of BIG thin film epitaxially grown on (111)-orientated GGG substrate. Experimental data and calculated curve are denoted by open circles and solid curve, respectively. (b) Wavelength dependence of the refractive index, n and extinction coefficient, k for the BIG thin film. These data were derived from the analysis of transmittance as shown in (a).

i.e., $k(\lambda) = (\lambda/4\pi)\exp[(1550/\lambda)^2 - 15.6]$, obtained from the calculation of the transmittance are illustrated in Fig. 7(b). It should be noted that n varies within only a narrow range from 2.44 to 3.20 in a broad wavelength range of 2000 to 200 nm whereas k increases drastically in the shorter wavelength region. At wavelengths longer than 500 nm, n is at least a hundred times larger than k. Our result of $n(\lambda)$, which is crucially important for the calculation of Faraday rotation, is in agreement with the fitting results reported by Dzibrou et al.,[40] Khartsev et al.,[41] and Deb et al.[42]

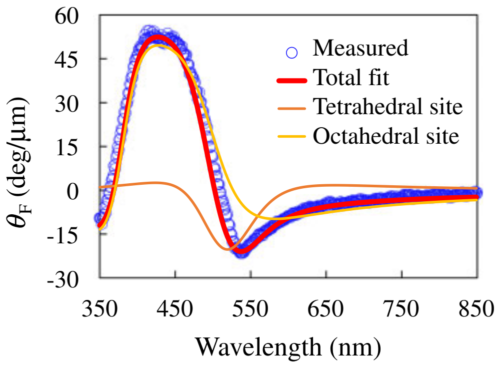

Fig. 8. (Color online) Experimental data (open circles) and calculated curve (solid curve) for wavelength dependence of Faraday rotation angle for the BIG thin film epitaxially grown on (111)-orientated GGG substrate. The contributions from Fe^{3+} ions at tetrahedral and octahedral sites are also presented.

Wavelength dependence of Faraday rotation angle experimentally obtained for the present BIG thin film is shown in Fig. 8; the data are denoted by open circles. A maximum and a minimum of Faraday rotation angle are observed in the wavelength region examined, with the former and the latter being at around 450 and 550 nm, respectively. Such a profile of the wavelength dependence of Faraday rotation angle is similar to those obtained for BIG thin films prepared by other methods. The largest Faraday rotation angle is $\theta_F = 54.3$ deg/μm at 424 nm and the negative rotation angle reaches −21.5 deg/μm at 538 nm. The value $\theta_F = 54.3$ deg/μm at 424 nm is comparable to but somewhat smaller than the largest value ever reported, i.e., 64 deg/μm at 2.92 eV (425 nm) for BIG thin film 220 nm thick prepared by PLD method.[42] This large value most likely comes from the fact that growth temperature as high as 950 K used in the PLD method improves the crystallinity of the PLD-derived BIG thin film. However, growth of single-phase BIG at such a high temperature is not accessible by the mist CVD method because BIG is converted into stable phases at growth temperatures higher than 550 °C. The Faraday rotation angle at 633 nm, at which the values of Faraday rotation angle were most frequently reported, for the present mist CVD-derived BIG is −7.2 deg/μm. The value is comparable to those of BIG thin films reported previously. For instance, $\theta_{F633nm} =$ −6.9, −5.3, and −6.7 deg/μm for BIG thin films prepared by RIBS, PLD, and MOD, respectively.[24,25,35] The magneto-optical figure of merit calculated from the data of Faraday rotation angle and normalized transmittance was found to be 13.3 deg at the wavelength of 532 nm. This value is larger by about 48% than that of BIG thin film prepared by PLD method.[43]

Faraday rotation angle θ_F is proportional to the imaginary part of the off-diagonal component of dielectric tensor ε_{xy} which can be calculated on the basis of quantum theory by assuming that $n \gg k$ in the wavelength range of interest and that two diamagnetic electric dipole transitions of Fe^{3+} ions at octahedral and tetrahedral sites (a- and d-sites) contribute to the Faraday effect in BIG.[44–49] The dispersion of Faraday rotation angle is given by

$$\theta_F(\omega) = -\frac{\omega}{2c}\frac{\varepsilon''_{xy}}{n} = -\frac{\pi e^2\omega^2}{2nmc}\sum_{i=a,d}\frac{Nf}{\omega_0}\left\{\frac{(\omega_0+\Delta)^2-\omega^2-\Gamma^2}{[(\omega_0+\Delta)^2-\omega^2+\Gamma^2]^2+4\omega^2\Gamma^2}-\frac{(\omega_0-\Delta)^2-\omega^2-\Gamma^2}{[(\omega_0-\Delta)^2-\omega^2+\Gamma^2]^2+4\omega^2\Gamma^2}\right\},$$

where e, m, c, ω, n, N, f, ω_0, 2Δ, Γ are the elementary charge, the electron mass, the velocity of light, the frequency of light, the refractive index of BIG thin film, the number density of absorption sites, the oscillator strength, the resonant frequency of electronic transition, the excited state splitting for the electronic transitions, and the full width at half maximum, respectively. We analyzed the experimental Faraday rotation angle as a function of wavelength by using this equation. The values of parameters, basically based on the crystal electric field (CEF) level schema for BIG proposed by Deb et al.[42] and used in the present analysis, are summarized in Table I. The calculated curve, shown as a solid curve in Fig. 8, agrees

Table I. Parameters used in the analysis of Faraday rotation as a function of wavelength for the BIG thin film epitaxially grown on (111)-oriented GGG substrate.

	$\hbar\omega_0$ (eV)	$\hbar\Delta$ (eV)	$\hbar\Gamma$ (eV)	Nf
Tetrahedral	2.38	0.075	0.31	-3.8×10^{23}
Octahedral	2.85	0.40	0.31	6.8×10^{23}

well with the experimental data, although a small discrepancy between them is detectable at wavelengths shorter than 550 nm, due to the considerable increase of extinction coefficient k in the wavelength range. The contributions from the tetrahedral and octahedral sites to the Faraday rotation are also illustrated in Fig. 8. It is revealed that the positive and negative rotation angles mainly stem from the electronic transitions of Fe^{3+} ions at octahedral and tetrahedral sites, respectively.

4. Conclusions

The thin film of single-phase BIG, known as a metastable garnet-type ferrite to manifest a large Faraday effect, was successfully synthesized by using the mist CVD method. The thin film was epitaxially grown on (111)-oriented single-crystalline GGG substrate under the conditions that the deposition was carried at 300 °C and the resultant amorphous thin film was post-annealed at 530 °C for 30 min. The BIG thin film thus obtained has a rather smooth surface as confirmed by AFM observation. The transmittance spectrum obtained experimentally is reproduced well in terms of a simple two-layer (thin film and substrate) model, suggesting that the thin film has a surface free from roughness with homogeneous thickness. The saturation magnetization reaches about 1620 G close to the value expected from the ideal magnetic structure of BIG. Also, the present BIG thin film manifests large Faraday effect; the maximum Faraday rotation angle is $\theta_F = 54.3\,\text{deg}/\mu\text{m}$ at a wavelength of 424 nm. The wavelength dependence of Faraday rotation angle observed experimentally can be quantitatively explained by considering electronic transitions of Fe^{3+} ions at both octahedral and tetrahedral sites. The present study proves that the mist CVD method is useful for the preparation of metastable complex oxides such as BIG.

Acknowledgement

This research was supported by JSPS KAKENHI Grants-in-Aid for Scientific Research (A) (No. 25249090), Scientific Research (B) (No. 24350104), and Challenging Exploratory Research (No. 26620192).

---

1) Y. Kajiwara, K. Harii, S. Takahashi, J. Ohe, K. Uchida, M. Mizuguchi, H. Umezawa, H. Kawai, K. Ando, K. Takanashi, S. Maekawa, and E. Saitoh, Nature **464**, 262 (2010).
2) A. A. Serga, A. V. Chumak, and B. Hillebrands, J. Phys. D **43**, 264002 (2010).
3) C. F. Buhrer, J. Appl. Phys. **40**, 4500 (1969).
4) H. Takeuchi, K. Shinagawa, and S. Taniguchi, Jpn. J. Appl. Phys. **12**, 465 (1973).
5) H. Takeuchi, S. Ito, I. Mikami, and S. Taniguchi, J. Appl. Phys. **44**, 4789 (1973).
6) S. Wittekoek and D. E. Lacklison, Phys. Rev. Lett. **28**, 740 (1972).
7) K. Shinagawa and S. Taniguchi, Jpn. J. Appl. Phys. **13**, 1663 (1974).
8) P. Hansen, W. Tolksdorf, K. Witter, and J. Robertson, IEEE Trans. Magn. **20**, 1099 (1984).
9) T. Okuda, N. Koshizuka, K. Hayashi, H. Taniguchi, K. Satoh, and H. Yamamoto, IEEE Transl. J. Magn. Jpn. **3**, 483 (1988).
10) A. Thavendrarajah, M. Pardavi-Horvath, and P. E. Wigen, IEEE Trans. Magn. **25**, 4015 (1989).
11) S. Mino, M. Matsuoka, A. Shibukawa, and K. Ono, Jpn. J. Appl. Phys. **29**, L1823 (1990).
12) B. M. Simion, G. Thomas, R. Ramesh, V. G. Keramidas, and R. L. Pfeffer, Appl. Phys. Lett. **66**, 830 (1995).
13) N. Adachi and T. Ota, J. Ceram. Soc. Jpn. **122**, 40 (2014).
14) T. Kawaharamura, H. Nishinaka, and S. Fujita, Jpn. J. Appl. Phys. **47**, 4669 (2008).
15) K. Kaneko, T. Nomura, I. Kakeya, and S. Fujita, Appl. Phys. Express **2**, 075501 (2009).
16) K. Kaneko, I. Kakeya, S. Komori, and S. Fujita, J. Appl. Phys. **113**, 233901 (2013).
17) S. Yao, T. Sato, K. Kaneko, S. Murai, K. Fujita, and K. Tanaka, Jpn. J. Appl. Phys. **53**, 05FB17 (2014).
18) E. A. Giess, D. C. Cronemeyer, R. Ghez, E. Klokholm, and J. D. Kuptsis, J. Am. Ceram. Soc. **56**, 593 (1973).
19) V. Babin, V. Gorbenko, A. Makhov, J. A. Mares, M. Nikl, S. Zazubovich, and Yu. Zorenko, J. Lumin. **127**, 384 (2007).
20) S. Leitenmeier, T. Körner, J. Griesbauer, M. Herbort, A. Heinrich, and B. Stritzker, J. Cryst. Growth **310**, 5392 (2008).
21) R. Lux, A. Heinrich, S. Leitenmeier, T. Körner, M. Herbort, and B. Stritzker, J. Appl. Phys. **100**, 113511 (2006).
22) J. B. Nelson and D. P. Riley, Proc. Phys. Soc. London **57**, 160 (1945).
23) T. Okuda, T. Katayama, H. Kobayashi, and N. Kobayashi, J. Appl. Phys. **67**, 4944 (1990).
24) N. Adachi, V. P. Denysenkov, S. I. Khartsev, A. M. Grishin, and T. Okuda, J. Appl. Phys. **88**, 2734 (2000).
25) M. Y. Chern and J. S. Liaw, Jpn. J. Appl. Phys. **36**, 1049 (1997).
26) S. Kahl, V. Popov, and A. M. Grishin, J. Appl. Phys. **94**, 5688 (2003).
27) E. Popova, L. Magdenko, H. Niedoba, M. Deb, B. Dagens, B. Berini, M. Vanwolleghem, C. Vilar, F. Gendron, A. Fouchet, J. Scola, Y. Dumont, M. Guyot, and N. Keller, J. Appl. Phys. **112**, 093910 (2012).
28) T. Kawaharamura, Jpn. J. Appl. Phys. **53**, 05FF08 (2014).
29) T. Yamashita and P. Hayes, Appl. Surf. Sci. **254**, 2441 (2008).
30) M. Y. Chern, F. Y. Lo, D. R. Liu, K. Yang, and J. S. Liaw, Jpn. J. Appl. Phys. **38**, 6687 (1999).
31) N. Adachi, T. Okuda, V. P. Denysenkov, A. Jalali-Roudsar, and A. M. Grishin, J. Magn. Magn. Mater. **242–245**, 775 (2002).
32) S. Mino, M. Matsuoka, A. Tate, A. Shibukawa, and K. Ono, Jpn. J. Appl. Phys. **31**, 1786 (1992).
33) B. Vertruyen, R. Cloots, J. S. Abell, T. J. Jackson, R. C. da Silva, E. Popova, and N. Keller, Phys. Rev. B **78**, 094429 (2008).
34) P. Hansen, K. Witter, and W. Tolksdorf, J. Appl. Phys. **55**, 1052 (1984).
35) N. Adachi, K. Isarai, T. Ota, K. Ishiyama, H. Ota, and K. Arai, Annu. Rep. Ceram. Res. Lab., Nagoya Inst. Technol. **10**, 1 (2010).
36) R. L. Comstock and P. E. Wigen, J. Appl. Phys. **36**, 2426 (1965).
37) R. Swanepoel, J. Phys. E **16**, 1214 (1983).
38) P. Johansson, S. I. Khartsev, and A. M. Grishin, Thin Solid Films **515**, 477 (2006).
39) T. Körner, A. Heinrich, M. Weckerle, P. Roocks, and B. Stritzker, J. Appl. Phys. **103**, 07B337 (2008).
40) D. O. Dzibrou and A. M. Grishin, J. Appl. Phys. **106**, 043901 (2009).
41) S. I. Khartsev and A. M. Grishin, J. Appl. Phys. **101**, 053906 (2007).
42) M. Deb, E. Popova, A. Fouchet, and N. Keller, J. Phys. D **45**, 455001 (2012).
43) S. Kang, S. Yin, V. Adyam, Q. Li, and Y. Zhu, IEEE Trans. Magn. **43**, 3656 (2007).
44) J. F. Dillon, Jr., in *Physics of Magnetic Garnets, Proc. Int. School of Physic: Enrico Fermi*, ed. A. Paoletti (North-Holland, Amsterdam, 1978) p. 379.
45) K. Shinagawa, in *Magneto-Optics*, ed. S. Sugano and N. Kojima (Springer, Berlin, 2000) p. 137.
46) L. E. Helseth, A. G. Solovyev, R. W. Hansen, E. I. Il'yashenko, M. Baziljevich, and T. H. Johansen, Phys. Rev. B **66**, 064405 (2002).
47) G. F. Dionne and G. A. Allen, J. Appl. Phys. **73**, 6127 (1993).
48) K. Matsumoto, S. Sasaki, K. Haraga, Y. Asahara, K. Yamaguchi, and T. Fujii, IEEE Trans. Magn. **28**, 2985 (1992).
49) S. Wittekoek, T. J. A. Popma, J. M. Robertson, and P. F. Bongers, Phys. Rev. B **12**, 2777 (1975).